

# TwinRL-VLA: Digital Twin-Driven Reinforcement Learning for Real-World Robotic Manipulation

Qinwen Xu<sup>1,\*</sup>, Jiaming Liu<sup>1,\*†</sup>, Rui Zhou<sup>4,\*</sup>, Shaojun Shi<sup>1,\*</sup>, Nuwei Han<sup>1,\*</sup>, Zhuoyang Liu<sup>1</sup>, Chenyang Gu<sup>1</sup>, Shuo Gu<sup>2</sup>, Yang Yue<sup>3</sup>, Gao Huang<sup>3</sup>, Wenzhao Zheng<sup>3</sup>, Sirui Han<sup>4</sup>, Peng Jia<sup>2</sup>, Shanghang Zhang<sup>1,✉</sup>

<sup>1</sup>State Key Laboratory of Multimedia Information Processing, School of Computer Science, Peking University  
<sup>2</sup>Simplexity Robotics <sup>3</sup>Tsinghua University <sup>4</sup>Hong Kong University of Science and Technology

Project page: <https://twinrl.github.io>

\*Equal Contribution †Project lead ✉Corresponding Author

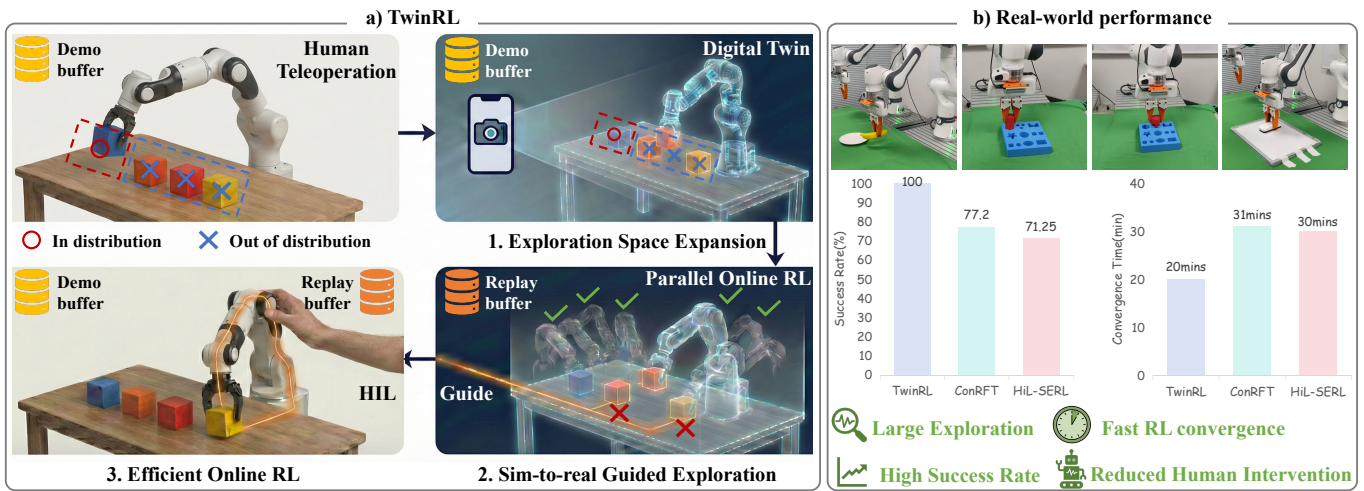


Fig. 1: **Overview.** (a) We propose **TwinRL**, a digital twin–real-world collaborative RL framework that expands the exploration space from in-distribution teleoperation data to out-of-distribution regions. TwinRL then performs efficient, parallel online RL in the digital twin to enable sim-to-real guided exploration, improving the convergence speed of real-world RL. (b) Across four tasks, TwinRL converges faster in online RL and approaches a 100% success rate, reaching this level in about 20 minutes on average in both in-distribution regions covered by real-world demonstrations and out-of-distribution regions. Since HiL-SERL does not include an SFT, its accuracy are reported only for the in-distribution region used by the other methods.

**Abstract**—Despite strong generalization capabilities, Vision-Language-Action (VLA) models remain constrained by the high cost of expert demonstrations and insufficient real-world interaction. While online reinforcement learning (RL) has shown promise in improving general foundation models, applying RL to VLA manipulation in real-world settings is still hindered by low exploration efficiency and a restricted exploration space. Through systematic real-world experiments, we observe that the effective exploration space of online RL is closely tied to the data distribution of supervised fine-tuning (SFT). Motivated by this observation, we propose TwinRL, a digital twin-real-world collaborative RL framework designed to scale and guide exploration for VLA models. First, a high-fidelity digital twin is efficiently reconstructed from smartphone-captured scenes, enabling realistic bidirectional transfer between real and simulated environments. During the SFT warm-up stage, we introduce an exploration space expansion strategy using digital twins to broaden the support of the data trajectory distribution. Building on this enhanced initialization, we propose a sim-to-

real guided exploration strategy to further accelerate online RL. Specifically, TwinRL performs efficient and parallel online RL in the digital twin prior to deployment, effectively bridging the gap between offline and online training stages. Subsequently, we exploit efficient digital twin sampling to identify failure-prone yet informative configurations, which are used to guide targeted human-in-the-loop rollouts on the real robot. In our experiments, TwinRL approaches 100% success in both in-distribution regions covered by real-world demonstrations and out-of-distribution regions, delivering at least a 30% speedup over prior real-world RL methods and requiring only about 20 minutes on average across four tasks.

## I. INTRODUCTION

Building on internet-scale pretrained Vision–Language Models (VLMs) [1, 21, 53], Vision–Language–Action (VLA) models have recently emerged as a promising paradigm for robotic manipulation [5, 22]. Through training on large-scale

robot demonstrations, VLA models have achieved encouraging progress in robotic scene reasoning [29, 30], open-world generalization [17, 31], and precise manipulation [3, 4]. Despite these advances, current VLA models remain constrained by their heavy reliance on expensive expert demonstrations and the limited amount of real-world interaction during training, which restricts robustness in complex physical environments.

Reinforcement learning (RL) provides an exploration-based framework that reweights cumulative task rewards, and has proven highly effective in enhancing the reasoning capabilities of general VLMs [45, 43, 46]. Motivated by this progress, recent studies have explored applying RL as a post-training stage for VLA models, leveraging offline RL updates [65, 16, 64] or online exploration in simulation [32, 50, 36, 14] to refine manipulation policies. While these approaches demonstrate that RL can improve execution accuracy, applying online RL to real-world robotic manipulation remains limited.

First, unlike simulation environments, real-world robots must engage in multi-round, safety-constrained interactions with physical objects, where parallel experimentation is infeasible, leading to severely limited efficiency for online learning [8]. Existing approaches enhance real-world RL efficiency through warm-up strategies [24, 26], unified training objectives [8], or human-in-the-loop (HiL) feedback mechanisms [39]. However, such approaches remain strongly dependent on the quality, diversity, and timing of teleoperated demonstrations, leading to unstable model convergence and inconsistent performance. Second, motivated by the general-domain study [62], which demonstrates that RL primarily reweights reasoning paths already supported by the base model rather than expanding them, we extend this insight to robotic manipulation. Through systematic real-world experiments, we observe that the effective exploration space of VLA models is closely tied to the data distribution used during supervised fine-tuning (SFT). Even with HiL assistance, learning in previously out-of-distribution (OOD) regions not covered by the SFT data remains challenging due to an unfavorable reward landscape and an imbalanced replay buffer. This observation exposes a critical bottleneck: although VLA models possess strong capacity, improving the exploration efficiency of real-world RL requires both expanding exploration support prior to online learning and actively guiding exploration.

To address this challenge, we propose TwinRL, a digital twin–real-world collaborative RL framework that enables bidirectional knowledge transfer between simulation and physical robots. As shown in Fig. 1 a), TwinRL is built upon the insight that digital twins can be leveraged not merely as simulators, but as exploration amplifiers and guides that systematically improve the efficiency of real-world RL. Specifically, we introduce an exploration space expansion strategy, in which diverse synthetic trajectories are generated within the digital twin to broaden exploration coverage during the SFT warm-up stage. In addition to augmented trajectories, paired real and synthetic samples under matched configurations are collected, facilitating alignment between real and simulated domains. To instantiate digital twins in novel environments, we reconstruct

high-fidelity scenes and objects from smartphone-captured videos using standard 3D Gaussian Splatting and convert them into mesh representations [61]. Within the digital twin, we estimate object-centric 6-DoF poses using AnyGrasp [11], providing an intermediate representation that bridges object motion and the end-effector control for constructing realistic manipulation trajectories.

Building upon this enriched warm-up, we propose a sim-to-real guided exploration strategy to further accelerate online RL. As shown in Fig. 1 a), TwinRL first performs efficient and parallel RL rollouts within the digital twin, generating online interaction data that are stored in a replay buffer. When applied to real-world RL, this strategy enriches the replay buffer with RL-style expert trajectories and bridges the transition from offline to online learning, reducing performance degradation and training instability. Moreover, replaying rollouts from well-performing configurations in the buffer prevents catastrophic forgetting of high-precision behaviors. In addition, the digital twin enables efficient identification of failure-prone yet informative object configurations, which are subsequently used to guide targeted HiL rollouts on the real robot, substantially accelerating exploration. As shown in Fig. 1 b), we evaluate TwinRL on four manipulation tasks, all built upon the same VLA backbone [41]. During the SFT stage, our exploration space expansion strategy improves average success by 42% compared to training solely on real-world demonstrations. During online RL, TwinRL achieves 100% success in both in-distribution regions covered by real-world demonstrations and OOD regions, delivering at least a 30% speedup over prior real-world RL methods [8, 39] and requiring only about 20 minutes on average across four tasks. Finally, the robustness of the TwinRL-trained policy is evaluated under previously unseen scenarios, such as background clutter and lighting variations. In summary, our contributions are as follows:

- We observe that exploration in real-world VLA RL is largely shaped by the trajectory distribution induced during SFT. Therefore, we propose **TwinRL**, a digital twin–real-world collaborative RL framework that leverages digital twins as exploration amplifiers and guides for efficient post-training.
- We introduce an exploration space expansion strategy that generates diverse trajectories within the digital twin to broaden exploration coverage, together with an efficient pipeline for constructing high-fidelity digital twins.
- We propose a sim-to-real guided exploration strategy to further accelerate online RL, which leverages efficient twin online rollouts to bridge the gap between offline and online learning, and efficiently guides targeted HiL exploration on real robots.

## II. RELATED WORK

**Vision-Language-Action (VLA)** models [22, 4, 27, 42, 31, 55, 6, 54, 34] ground high-level language instructions into visuomotor control, enabling robots to accomplish tasks in dynamic environments. To effectively model precise robotic actions, recent works typically couple VLM representations with

specialized action experts, such as diffusion-based heads [33, 54, 27, 3, 63, 18, 13] that generate actions via iterative denoising, or flow-based [4, 17, 48] formulations for efficient generative modeling. While VLA policies are trained through supervised fine-tuning (SFT), their reliance on static demonstration data limits broader state exploration.

**Reinforcement Learning (RL) for VLA models.** RL policies can continue to improve robustness post-deployment through online interaction and feedback from the environment [50]. Existing RL post-training approaches for VLAs follow two primary paradigms. Offline methods [65, 64] optimize policies using fixed trajectories or preference data to enhance alignment and robustness. Alternatively, online approaches [36, 50, 9, 14, 8] leverage interactive simulator rollouts and iterative updates to improve task performance and stability. Recent work has started to bring *real-world* RL to physical robots by training policies directly through on-robot interaction, often leveraging human-in-the-loop feedback and safety-aware data collection to improve sample efficiency [39, 8, 37, 40, 25, 38]. However, they typically require extensive real-world interaction and prolonged training, which are costly, low-throughput, and further constrained by safety risks. SimLauncher [56] uses a digital-twin-pretrained policy to bootstrap critic learning with simulated and real-world demonstrations, and to provide action proposals during RL. In this paper, we systematically analyze how the SFT data distribution constrains policy exploration and propose a high-fidelity digital twin to expand the effective exploration space and improve exploration efficiency during joint simulation and real-world post-training.

**Digital Twin-Based Sim-to-Real Data Scaling.** To generate more training data from limited real demonstrations while mitigating the sim-to-real gap, many works [60, 35, 59, 57, 58] adopt a Real2Sim2Real paradigm built upon a digital twin. DexMimicGen [20] supports demonstration-based policy learning by reusing and organizing assets in simulation. RoboVerse [12] provides larger-scale simulated interactions to promote general manipulation. RialTo [52] and CASHER [51] integrate real observations with interactive simulation components for policy optimization. RoboGSim [28] combines 3D Gaussian Splatting with a physics engine to enable scalable real2sim2real data generation and strong sim-to-real transfer. Real2Render2Real [61] uses a phone scan and one human video to render large-scale robot training demos via 3D Gaussian Splatting, avoiding teleoperation and dynamics simulation. Additionally, GSWorld [19] enables closed-loop, photo-realistic simulation by combining 3D Gaussian Splatting with physics for reproducible evaluation and sim-to-real policy learning. Unlike prior work, we innovatively leverage a digital twin for both scalable data generation and online exploration, systematically serving as an exploration amplifier and guide for efficient real-world RL.

### III. METHOD

#### A. Preliminary

**Vision-Language-Action (VLA) Policy Action Generation.** The VLA policy  $\pi_\theta$  maps a language instruction  $\ell$  and multi-

view images  $I_t = \{I_t^{\text{side}}, I_t^{\text{wrist}}\}$  to a 7-DoF end-effector action  $a_t \sim \pi_\theta(a_t | I_t, \ell)$  at each timestep  $t$ . The action  $a_t = (\Delta p_t, \Delta r_t, g_t)$  defines the relative movement of the end-effector, comprising a 3D translational delta  $\Delta p_t \in \mathbb{R}^3$ , a 3D rotational change  $\Delta r_t \in \mathbb{R}^3$ , and a binary gripper state  $g_t \in \{0, 1\}$ . We denote a rollout trajectory as  $\tau = \{(I_t, \ell, a_t)\}_{t=1}^T$ , which terminates upon task success or reaching a time limit.

**Reinforcement Policy.** Following previous works [8, 39], reinforcement learning (RL) serves as an interactive post-training paradigm that leverages environmental feedback to optimize fine-grained manipulation and broaden state coverage through exploration. Robotic RL can be formulated as a Markov decision process (MDP)  $\mathcal{M} = \{\mathcal{S}, \mathcal{A}, \rho, \mathcal{P}, r, \gamma\}$ , where  $s \in \mathcal{S}$  denotes the state observation,  $a \in \mathcal{A}$  denotes the action,  $\rho(s_0)$  is the initial-state distribution,  $\mathcal{P}$  is the unknown and potentially stochastic transition dynamics,  $r : \mathcal{S} \times \mathcal{A} \rightarrow \mathbb{R}$  is the reward function, and  $\gamma \in (0, 1]$  is the discount factor. Under this setting, to evaluate the performance of a policy  $\pi$ , we define the state-value function as

$$V^\pi(s) = \mathbb{E}_\pi \left[ \sum_{t=0}^H \gamma^t r(s_t, a_t) \mid s_0 = s \right], \quad (1)$$

and the action-value function is defined as

$$Q^\pi(s, a) = \mathbb{E}_\pi \left[ \sum_{t=0}^H \gamma^t r(s_t, a_t) \mid s_0 = s, a_0 = a \right], \quad (2)$$

which satisfy  $V^\pi(s) = \mathbb{E}_{a \sim \pi(\cdot | s)} [Q^\pi(s, a)]$ . We define the optimal policy  $\pi^*$  as the one maximizing the expected return over trajectories  $\tau$  sampled from the distribution of  $(\rho, \mathcal{P}, \pi)$ :

$$\pi^* = \arg \max_\pi \mathbb{E}_\pi \left[ \sum_{t=0}^H \gamma^t r(s_t, a_t) \right]. \quad (3)$$

$\pi_\theta(a|s)$  is parameterized by a neural network and can be modeled as a Gaussian distribution for continuous control.

#### B. Motivation

While online RL provides an exploration pathway toward task robustness, its sample efficiency on physical hardware remains a challenge. Motivated by the general-domain study [62], we observe that exploration in real-world VLA RL is effectively constrained by the spatial support of the trajectory distribution induced during SFT. This constraint introduces a dual bottleneck: (1) it limits the set of states that can be reliably explored, and (2) it substantially reduces online RL efficiency, even with human intervention.

**Experimental Setup.** In Fig. 2 (a), we conduct all experiments using a precision block insertion task that requires high positional accuracy. All policies are instantiated based on the Octo [41] model. We partition the workspace into an in-distribution Region A, which is covered by demonstrations, and an out-of-distribution (OOD) Region B that is not observed during SFT.

**Bottleneck I.** The spatial coverage of SFT demonstrations is varied to isolate its impact on policy generalization and

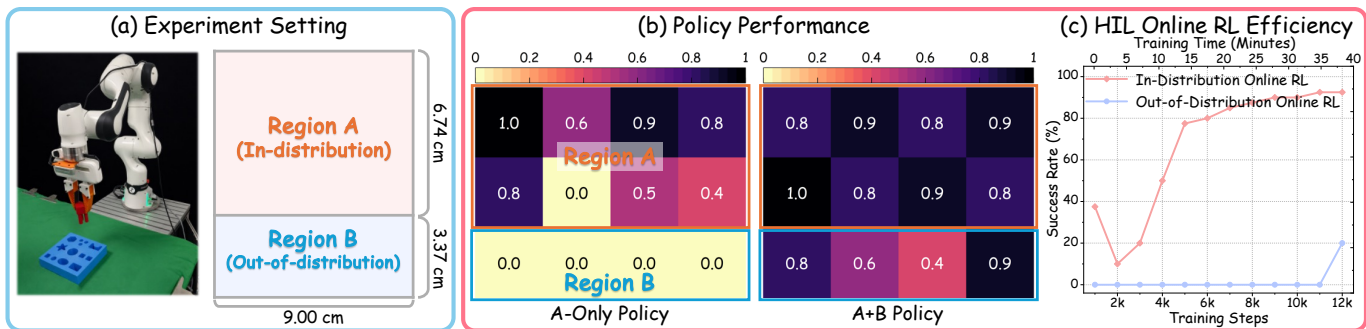


Fig. 2: **Exploration Bottlenecks.**(a) We split the workspace into an in-distribution region (A) and an OOD region (B). Each region is defined by the manipulated object’s center location at task completion. (b) Heatmaps visualize the performance of different policies. (c) Learning curves show the online RL training dynamics of the A-only policy in both regions.

autonomous online RL. Specifically, we compare two training data distributions: (i) **A-only**, with 30 demonstrations from Region A, and (ii) **A+B**, which adds 30 digital-twin demonstrations from Region B. We first evaluate the spatial generalization of the resulting SFT policies. To measure how demonstration coverage shapes the effective exploration space, we initialize the policy with the A-only SFT model and run autonomous online RL in the unseen Region B.

**Findings I.** As shown in Fig. 2(b), we perform 10 rollouts within each grid cell. In Region B, the **A+B** policy achieves a success rate of 62.5%, whereas the **A-only** policy remains confined to Region A (0% in Region B). This result indicates that standard SFT policies exhibit limited extrapolation to spatially uncovered regions. More importantly, attempting autonomous online RL in Region B from the **A-only** model leads to a pronounced exploration deadlock. When initialized in OOD configurations, the policy fails to consistently obtain positive rewards, even after 40K training steps (approximately two hours). This phenomenon is similar to [8], where the replay buffer becomes dominated by failure trajectories and autonomous adaptation is rendered practically ineffective. These results show that, consistent with findings in the general-domain work [62], the effective exploration space of online RL is closely tied to the spatial coverage of the SFT data.

**Bottleneck II.** To mitigate the exploration deadlock, Human-in-the-Loop (HiL) intervention can be introduced to guide the robot toward successful task completion [39]. However, an important question remains: does the availability of human guidance guarantee efficient online adaptation in OOD settings? To examine this, we compare two settings: **In-distribution Post-training**, where online RL is performed in the familiar Region A, and **OOD Post-training**, where online RL is conducted in the unfamiliar Region B. All models are initialized from the same A-only SFT policy.

**Findings II.** Despite human interventions providing successful corrective demonstrations in both settings, we observe a pronounced disparity in sample efficiency. As shown in Fig. 2 (c), in-distribution post-training adapts rapidly, achieving over 90% success within approximately 45 minutes ( $\sim 14k$  interaction steps). In contrast, OOD post-training converges substan-

tially more slowly and exhibits greater instability under the same interaction budget, failing to reach comparable performance. These results indicate that, even with the incorporation of a HiL scheme, learning in the previously unseen Region B remains challenging due to an unfavorable reward landscape and an imbalanced data distribution in the data buffer, both of which substantially reduce gradient efficiency.

**Conclusion.** These observations suggest that overcoming both bottlenecks requires expanding exploration coverage *before* real-world interaction and guiding human intervention to systematically improve online efficiency. Motivated by this, we propose **TwinRL**, a digital twin–real-world collaborative RL framework that uses digital twins as efficient exploration amplifiers and guides during both SFT and online RL stages. Additional motivation experiments on exploration in other tasks are provided in Appendix A.

### C. Exploration Space Expansion Strategy

**Digital Twin Construction.** We construct a high-fidelity digital twin of the target manipulation environment as the primary substrate for *exploration-prior expansion* in TwinRL. It is rapidly instantiated from casually captured smartphone videos by reconstructing the scene using 3DGS tools [23] (about 10 minutes), the manipulable objects using SAM3D [7] (about 5 seconds), and the robot from its URDF model. All components are unified as mesh-based assets for kinematic assembly and efficient rendering in Blender. To enable bidirectional knowledge transfer, we align the digital twin with the real environment at both the visual and robot-state levels. Alignment is anchored to URDF-defined robot frames: we obtain a coarse match via point-cloud registration (e.g., ICP [2]) and refine it with differentiable 3DGS rendering [59] to align rendered and real observations, yielding consistent coordinate frames. Rather than full physics simulation, the digital twin uses a kinematic interaction model that prioritizes visual–geometric consistency [61]. We adopt an object-centric representation by estimating the manipulated object’s 6-DoF grasp pose with AnyGrasp [11], defining the object and end-effector relationship. Starting from a single successful object trajectory, we generate diverse execution trajectories via

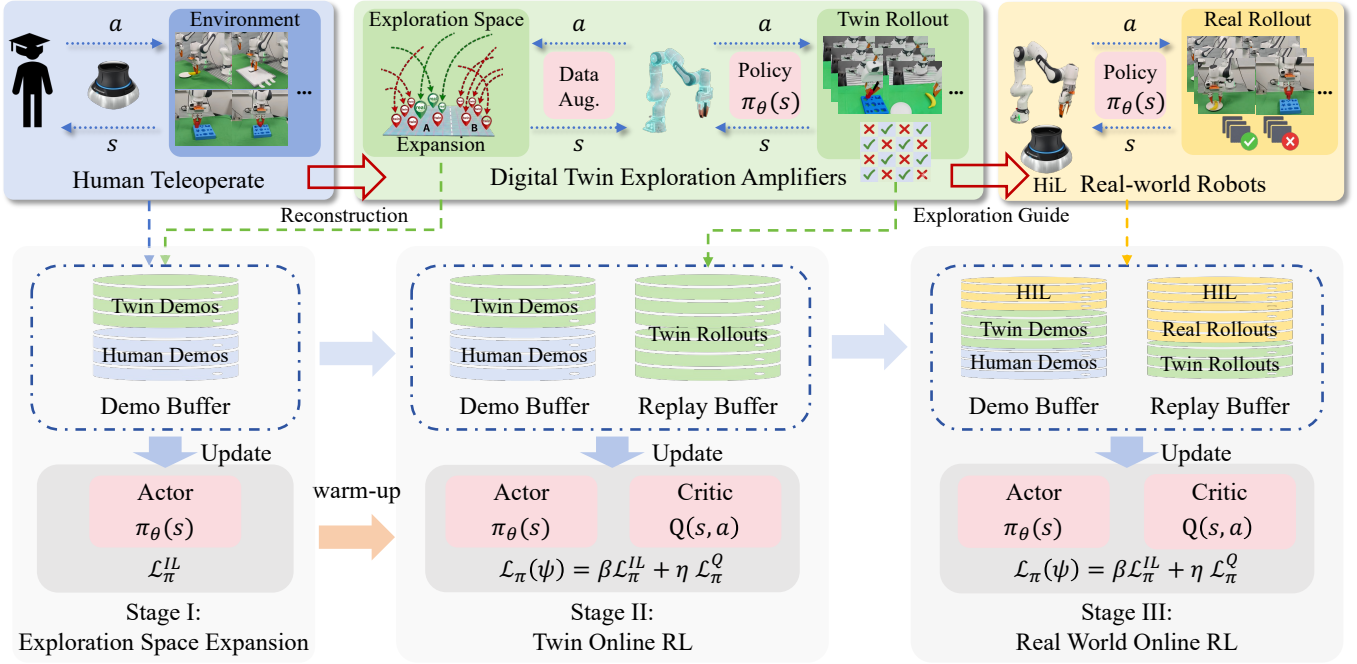


Fig. 3: **TwinRL**. Stage I: Starting from human teleoperation, we introduce an exploration-space expansion strategy that synthesizes diverse digital-twin demonstrations to broaden SFT coverage. Stage II: The SFT-initialized policy is then trained with scalable, parallel online RL in the digital twin to harvest RL-style rollouts, which are transferred to initialize the real-world replay buffer and stabilize online learning. Stage III: During real-world online RL, the digital twin efficiently and continuously identifies failure-prone yet informative object configurations, which are then used to guide targeted HiL rollouts.

inverse kinematics, motion planning, or affine transformations. Details are provided in Appendix C.

**Exploration Amplifiers.** During the warm-up stage, we treat the digital twin as an *exploration amplifier*, enriching trajectory diversity to expand the effective exploration space for subsequent online RL. As shown in Fig. 3 Stage I, we generate diverse object-centric synthetic trajectories that go beyond real demonstrations by varying the object’s initial configurations, target poses, and motion paths. Given an object’s initial pose  $T_0 \in SE(3)$  and a desired target pose  $T_{\text{target}} \in SE(3)$ , we estimate a task-consistent grasp pose  $T_{\text{grasp}}$  and derive the boundary end-effector poses:

$$T_{\text{start}}^{\text{ee}} = T_0 \cdot T_{\text{grasp}}, \quad T_{\text{end}}^{\text{ee}} = T_{\text{target}} \cdot T_{\text{grasp}}. \quad (4)$$

The intermediate trajectory is generated via motion planning or by applying affine transformations to a single demonstration trajectory, ensuring trajectory quality. Note that for a 30-step task, with parallel processing, we only need about 1 minute to construct a set of digital-twin demonstrations. To internalize these augmented behaviors, we perform an SFT stage on the merged buffer  $\mathcal{D}$  by minimizing the imitation learning loss:

$$\mathcal{L}_\pi^{\text{IL}} = -\mathbb{E}_{(s, a) \sim \mathcal{D}}[\log \pi_\psi(a|s)]. \quad (5)$$

We use the digital twin not only to mitigate exploration deadlock in OOD regions, but also to collect additional in-distribution data, thereby narrowing the sim-to-real gap.

#### D. Sim-to-Real Guided Exploration

Although our approach expands the exploration support of the VLA model during the SFT stage, directly launching online RL on real robots remains non-trivial due to two critical bottlenecks. First, the distribution mismatch between supervised demonstrations  $\mathcal{D}_{\text{sft}}$  and the RL-style expert trajectories  $\mathcal{D}_{\text{rl}}$  can cause severe performance degradation and  $Q$ -value instability during the offline-to-online transition. Second, HiL-guided online RL still incurs high sample complexity and relies heavily on human operator expertise. To address these challenges, we leverage the digital twin as a parallel compute engine and introduce a twin online RL stage together with a failure-aware exploration mechanism, transforming real-world exploration into a more targeted and sample-efficient process.

**Twin Online RL Stage.** As shown in Fig. 3 Stage II, to bridge the distribution gap between demonstration data and RL-style interaction data, we first perform parallel online RL in the digital twin. In this stage, the policy  $\pi_\psi$  is initialized from the SFT model and trained through interaction with  $N$  parallel twin environments. Inspired by ConRFT [8], we adopt a joint objective that combines RL with an imitation-based regularization term to stabilize policy updates during twin-based online interaction. The objective is defined as:

$$\mathcal{L}_\pi^{\text{twin}}(\psi) = \beta \mathcal{L}_\pi^{\text{IL}} + \eta \mathcal{L}_\pi^{\text{Q}}, \quad (6)$$

where  $\mathcal{L}_\pi^{\text{IL}}$  is the same loss used in SFT, and  $\mathcal{L}_\pi^{\text{Q}} = -\mathbb{E}_{s \sim \mathcal{D}, a \sim \pi_\psi(\cdot|s)}[Q_\theta(s, a)]$  is an RL objective that encour-

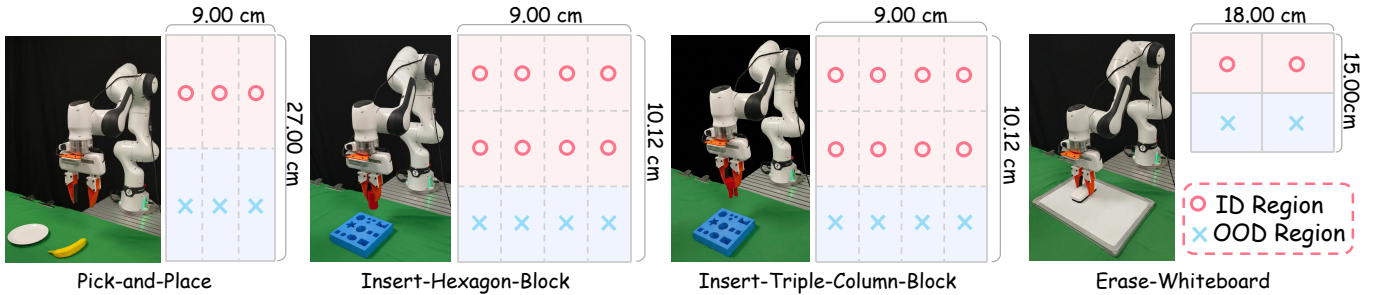


Fig. 4: **Real-world experimental setup.** We consider four tasks, namely Pick-and-Place, Insert-Hexagon-Block, Insert-Triple-Column-Block, and Erase-Whiteboard, covering multi-step, precise, and contact-rich manipulation. The red and blue areas denote the in-distribution (ID) and out-of-distribution (OOD) evaluation regions, respectively.

ages actions with higher critic-estimated  $Q$  values [15]. The value function  $Q_\theta$  is updated via standard temporal-difference learning. Through this process, the twin online RL stage efficiently collects diverse trajectories  $\tau_{\text{twin}}$ , including successful executions, failures, and recovery behaviors, which are stored in the twin replay buffer  $\mathcal{D}_{\text{twin}}$ . Note that parallel processing enables us to generate a set of rollouts in about 1 minute (e.g., 30 steps per episode). Due to the distribution gap between demonstration data and RL-style interaction data, early online learning may exhibit instability. Therefore, after efficient online learning in the digital twin, the real-world replay buffer is initialized with data transferred from the twin buffer  $\mathcal{D}_{\text{real}}^{\text{init}} \leftarrow \mathcal{D}_{\text{twin}}$ . By providing more balanced training signals, the replay buffer reduces training instability and mitigates performance degradation during the initial training phase when transitioning from offline SFT to real-world online learning. Moreover, this strategy helps prevent catastrophic forgetting in configurations that already exhibit strong performance during subsequent targeted HiL-guided online RL.

**Real-world online RL.** As shown in Fig. 3 Stage III, we leverage the digital twin to identify failure-prone regions of the state space and guide the initial-state distribution for real-world online RL. Unlike prior curriculum or reset-based strategies that rely on real-world rollouts [39], the digital twin enables low-cost and systematic evaluation of policy performance across a wide range of initial configurations without consuming physical interaction budget. Specifically, we evaluate the current policy in the digital twin and construct a targeted set of initial configurations,  $\mathcal{S}_{\text{target}} = \{s_0 \mid SR(s_0) < \tau\}$ , where  $SR(s_0)$  denotes the empirical success rate from state  $s_0$ , and  $\tau$  is a proficiency threshold. During real-world online interaction, episode resets are prioritized from  $\mathcal{S}_{\text{target}}$ , enabling the learning process to focus limited physical interaction budget on challenging states. To further reduce the cost and risk of exploration in challenging regions, we incorporate a HiL mechanism during real-robot training [39]. The resulting intervention trajectories are stored in the replay buffer and used for subsequent policy updates. Unlike existing HiL-based approaches, we introduce a novel guidance mechanism in which the digital twin informs where and when HiL intervention should be applied during real-world RL.

## IV. EXPERIMENT AND RESULTS

We first detail the experimental setup in Section IV-A, followed by extensive real-world comparisons against baselines in Section IV-B. Each component of TwinRL is then ablated in Section IV-C, and robustness is evaluated in Section IV-D under varying backgrounds and lighting conditions.

### A. Experimental Setup

**Hardware Platforms.** For real-world manipulation, we conduct systematic experiments on a 7-DoF Franka Emika Research 3 (FR3) robot. Our setup features a dual-camera perception system, comprising a fixed third-person view for global context and a wrist-mounted camera for fine-grained details.

**Experiment Protocol.** As shown in Fig. 4, we discretize each task workspace into a grid, and assign each episode to a grid cell based on the manipulated object’s center location at task completion. In the figure, the red area denotes (1) in-distribution (ID) regions covered by the collected real-world demonstrations, while the blue area denotes (2) out-of-distribution (OOD) regions that are not covered by real-world data. Although we augment SFT with digital-twin data covering both ID and OOD regions, our goal is to demonstrate that a digital twin can serve as an efficient amplifier and guide for online RL in regions not covered by real-world data. More details of the setup are provided in Appendix B.

### B. Real-World Experiments

**Implementation Details and Baselines.** To ensure a fair comparison, we strictly control real-world demonstration data usage across all methods. **HiL-SERL** [39] deploys the policy directly onto the physical robot to perform Human-in-the-Loop (HiL) online RL training. **ConRFT** [8] serves as a strong baseline utilizing 30 real-world demonstrations from the ID region; it first undergoes the first-stage Cal-ConRFT [8], followed by HiL online RL fine-tuning in the real world. All loss supervision follows the official paper. **Our method** uses the same 30 real-world demonstrations and further leverages the digital twin as an exploration amplifier by adding 60 synthetic trajectories in the ID region and 30 synthetic trajectories covering the OOD region. We report two variants: TwinRL w/o buffer and TwinRL. They differ in whether a twin replay buffer, collected via parallel online RL in the digital twin, is

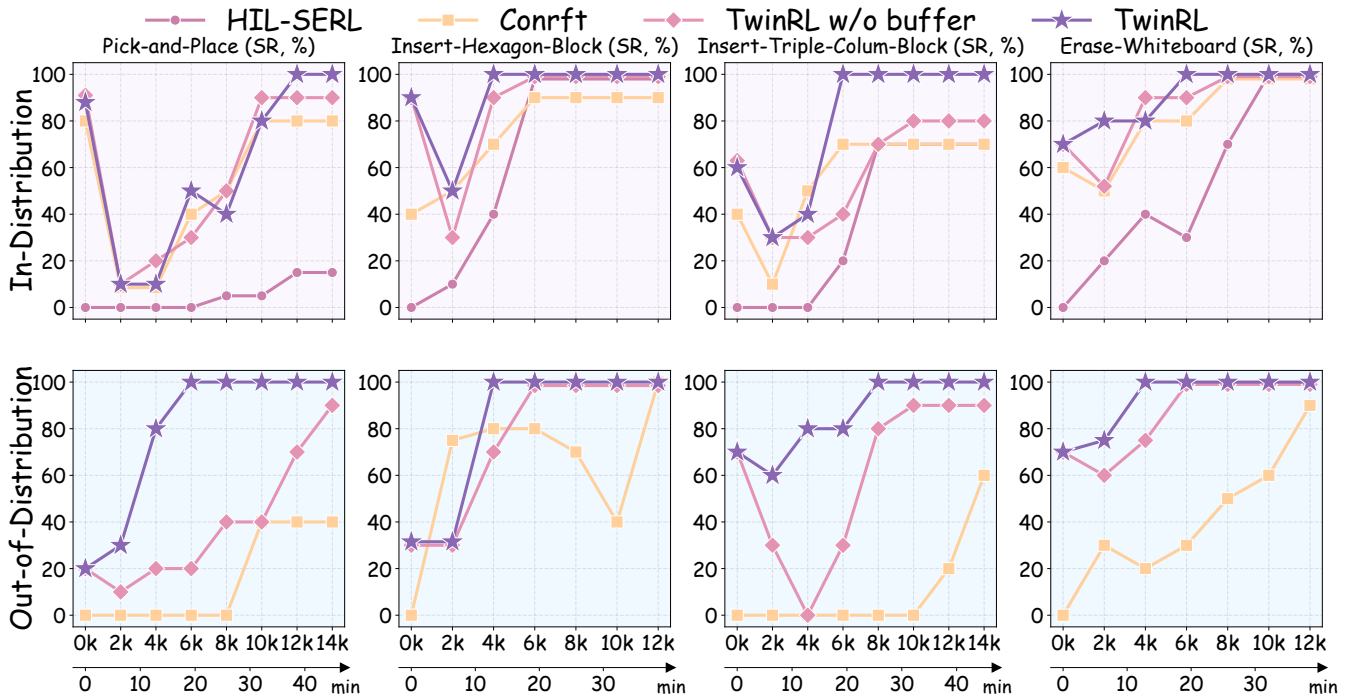


Fig. 5: **Real-world Experiments.** We report success-rate curves for online RL across four manipulation tasks under both ID and OOD settings. The y-axis shows success rate, and the x-axis reports both online training time and our model training steps.

TABLE I: **Ablation on exploration space expansion.** We vary the number of twin-generated trajectories added during SFT warm-up and measure the resulting success rate (SR).

Data volume		In-Distribution	Out-of-Distribution	Avg.
In	Out	SR ( $\uparrow \Delta$ )	SR ( $\uparrow \Delta$ )	SR ( $\uparrow \Delta$ )
0	0	40%	0%	27%
30	30	70% (+30%)	30% (+30%)	57% (+30%)
60	30	<b>80% (+40%)</b>	40% (+40%)	<b>67% (+40%)</b>
30	60	70% (+30%)	<b>70% (+70%)</b>	70% (+43%)

TABLE II: **Ablation on the twin buffer.** We report success rate and RL training steps. **S** denotes successful trajectories, and **F** denotes failed trajectories.

Ablation	Setting	Online Steps	Success Rate
Twin Buffer	0 S / 0 F	5.0k	90%
	20 S / 0 F	<b>3.5k</b>	<b>100%</b>
	30 S / 0 F	4.0k	90%
	20 S / 20 F	4.5k	90%
	20 S / 40 F	7.0k	70%

used to initialize training before real-world HiL online RL. For all methods, we evaluate each region with at least 10 randomly sampled rollout trials.

**Metrics and Results** We report success rate (SR) as a function of real-world training time and training steps to compare convergence speed and final performance in both ID and OOD regions. Figure 5 summarizes the online training curves across four tasks. **Initialization** (0-step). TwinRL starts with substantially higher SR at the onset of real-world online RL (i.e., before any real interaction). This gain is attributed to the exploration space expansion during SFT, where digital-twin trajectories broaden the support of the pretraining distribution and yield a stronger deployment prior. **In ID regions**, the key difference between TwinRL and the baselines lies in whether sim-to-real guided exploration is available. Most TwinRL variants exceed 90% SR and converge noticeably faster than the baselines, indicating that our digital-twin online rollout strategy serves as an effective guide for real-world RL. By efficiently identifying informative object configurations in the twin, TwinRL focuses HiL interactions on

high-value states, accelerating convergence while maintaining high execution accuracy. **In OOD regions**, the gap is more pronounced. TwinRL attains high SR with far fewer real-world interactions, whereas ConRFT and HiL-SERL converge more slowly or fail to reach comparable performance under the same interaction budget. This demonstrates that TwinRL effectively expands exploration beyond the spatial support of real demonstrations and enables rapid adaptation to previously unseen configurations. **Stability.** Finally, all methods exhibit noticeable SR degradation when transitioning from offline SFT to online learning, indicating instability under the distribution shift from SFT to RL-style data. TwinRL minimizes this gap and recovers performance much faster, reaching 100% SR. This improved stability is consistent with transferring twin RL rollouts to initialize the real replay buffer, which bridges the offline-to-online transition and mitigates early-stage performance collapse. Failure analysis is provided in Appendix E. Additional quantitative results and visualizations are provided in Appendix D and the project page.

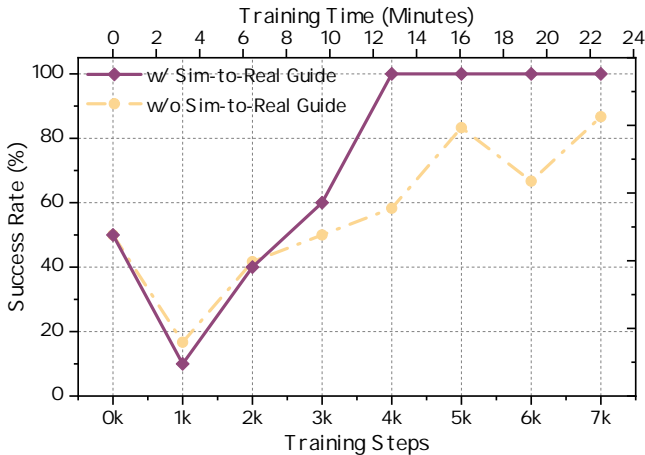


Fig. 6: **Ablation on Sim-to-Real-Guided HiL.** The guidance markedly accelerates RL learning, reaching 100% success at around 4k steps ( $\sim 14$  min), while training without guidance improves more slowly and attains a lower success rate.

### C. Ablation Study

We select Insert-Hexagon-Block for ablation. As shown in Fig. 4, we perform 10 rollout trials for each row.

**Impact of Exploration Space Expansion.** We analyze how the scale and distribution of twin data affect warm-up performance. Table I reports success rates under different ID/OOD synthetic-trajectory augmentations. Compared to the base model, a balanced setting with 30 ID and 30 OOD twin trajectories achieves 57.0% SR (+30%), indicating that our digital-twin pipeline can generate high-quality trajectories across the workspace even for the precision-critical task. Increasing the amount of twin data further improves performance: doubling ID data (60/30) yields the largest gain, reaching a peak ID SR of 80%, while increasing OOD data (30/60) improves SR to 70%. Overall, these results confirm that our exploration space expansion strategy effectively broadens SFT coverage. More synthetic data can further help, but it also increases SFT time, creating an accuracy–efficiency trade-off.

**Impact of twin RL replay buffer.** Next, we study how the composition of the twin replay buffer affects the efficiency and stability of online RL. Specifically, we vary the ratio of successful to failed twin rollouts stored in the buffer, ranging from success-only buffers to buffers with an increasing number of failure examples. As shown in Table II, most settings ultimately reach over 90% success in both ID and OOD regions. Taken together with Fig. 5, these results show that seeding the twin buffer with successful trajectories can substantially accelerate online RL training. However, adding more failure rollouts reduces online RL efficiency, contrary to our expectation. We attribute this to the fact that failure trajectories sampled from the digital twin often reflect random failure modes rather than meaningful, task-relevant failures encountered during real-world HiL interaction, and thus do not effectively teach the policy to avoid failure states. In future work, we will explore more principled ways to incorporate

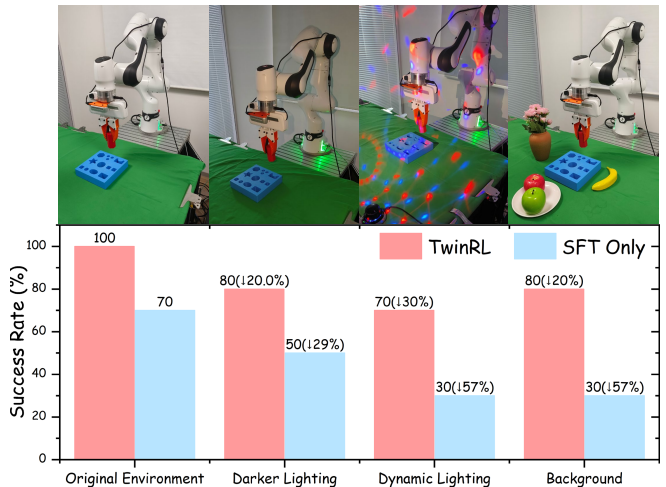


Fig. 7: **Robustness.** We compare the SFT policy and the TwinRL-guided online RL policy under previously unseen environmental perturbations; the top row shows examples.

informative failures before online RL.

**Efficiency of Sim-to-Real-Guided HiL.** Finally, we evaluate the role of digital-twin-guided HiL during real-world online RL. As shown in Fig. 6, we compare TwinRL with and without the proposed guidance mechanism, which uses digital-twin rollouts to identify informative initial object configurations and trigger HiL intervention when necessary. The results show that enabling twin-guided intervention significantly reduces the number of real-world training steps required, achieving faster convergence while maintaining a higher success rate. In contrast, removing the guidance mechanism leads to slower adaptation and lower sample efficiency, despite using the same policy parameter initialization and replay buffer. These results demonstrate that digital twins in TwinRL not only expand exploration support prior to deployment but also play a critical role during online learning by steering real-world interaction toward challenging yet informative regions of the state space. Due to space limitations, additional ablation studies are provided in Appendix D.

### D. Robustness Analysis

We compare the SFT policy and the TwinRL-guided online RL policy under a zero-shot robustness evaluation with previously unseen environmental perturbations, including background clutter and lighting variations. As shown in Fig 7, we consider three test conditions: Background (adding task-irrelevant objects to create clutter), Darker lighting (uniform illumination changes), and Dynamic lighting (dynamic colored lighting with moving light patterns). All perturbations are applied to the hexagonal block insertion task. The results show that, despite the observation distribution shift, TwinRL suffers only a minor performance drop, whereas the SFT-only model exhibits a substantially larger degradation. The results demonstrate that, through real-world interaction, RL fine-tuning pushes the policy toward more stable control and noise-tolerant decision boundaries. TwinRL further improves

robustness by using twin-guided HiL to concentrate real-world interactions on high-information configurations.

## V. CONCLUSION AND LIMITATION

In this work, we identify a critical bottleneck in real-world VLA RL: the effective exploration space is largely shaped by the trajectory distribution induced during SFT, making adaptation in regions not covered by SFT data difficult even with HiL. To address this, we present TwinRL, our first attempt to construct a high-fidelity digital twin not merely as a simulator, but as an exploration amplifier and guide for real-world online RL. TwinRL combines (i) an exploration-space expansion warm-up that synthesizes diverse trajectories in the twin to broaden SFT coverage, and (ii) sim-to-real guided exploration that uses parallel twin RL rollouts to seed the real replay buffer and identify informative, failure-prone configurations for targeted HiL interventions. Experiments across four real-world manipulation tasks show that TwinRL substantially improves sample efficiency and robustness. We hope TwinRL provides a practical and novel pathway toward deploying online RL on physical robots.

Although TwinRL partially mitigates the offline-to-online transition gap, a residual performance gap can still arise in the early stages due to unavoidable distribution shift. Future work will explore more principled sim-to-real guidance and better use of informative twin RL trajectories to further reduce reliance on HiL and improve early-stage stability.

## REFERENCES

- [1] Jean-Baptiste Alayrac, Jeff Donahue, Pauline Luc, Antoine Miech, Iain Barr, Yana Hasson, Karel Lenc, Arthur Mensch, Katherine Millican, Malcolm Reynolds, et al. Flamingo: a visual language model for few-shot learning. *Advances in Neural Information Processing Systems*, 35: 23716–23736, 2022.
- [2] Paul J Besl and Neil D McKay. Sensor fusion iv: control paradigms and data structures. *International Society for Optics and Photonics*, 1611:586–607, 1992.
- [3] Johan Bjorck, Fernando Castañeda, Nikita Cherniadev, Xingye Da, Runyu Ding, Linxi Fan, Yu Fang, Dieter Fox, Fengyuan Hu, Spencer Huang, et al. Gr00t n1: An open foundation model for generalist humanoid robots. *arXiv preprint arXiv:2503.14734*, 2025.
- [4] Kevin Black, Noah Brown, Danny Driess, Adnan Esmail, Michael Equi, Chelsea Finn, et al. pi0: A vision-language-action flow model for general robot control. *arXiv preprint arXiv:2410.24164*, 2024.
- [5] Anthony Brohan, Noah Brown, Justice Carbajal, Yevgen Chebotar, Xi Chen, Krzysztof Choromanski, Tianli Ding, Danny Driess, Avinava Dubey, Chelsea Finn, et al. Rt-2: Vision-language-action models transfer web knowledge to robotic control. In *arXiv preprint arXiv:2307.15818*, 2023.
- [6] Hao Chen, Jiaming Liu, Chenyang Gu, Zhuoyang Liu, Renrui Zhang, Xiaoqi Li, Xiao He, Yandong Guo, Chi-Wing Fu, Shanghang Zhang, et al. Fast-in-slow: A dual-system foundation model unifying fast manipulation within slow reasoning. *arXiv preprint arXiv:2506.01953*, 2025.
- [7] Xingyu Chen, Fu-Jen Chu, Pierre Gleize, Kevin J Liang, Alexander Sax, Hao Tang, Weiyao Wang, Michelle Guo, Thibaut Hardin, Xiang Li, et al. Sam 3d: 3dfy anything in images. *arXiv preprint arXiv:2511.16624*, 2025.
- [8] Yuhui Chen, Shuai Tian, Shugao Liu, Yingting Zhou, Haoran Li, and Dongbin Zhao. Conrft: A reinforced fine-tuning method for vla models via consistency policy. *arXiv preprint arXiv:2502.05450*, 2025.
- [9] Zengjue Chen, Runliang Niu, He Kong, Qi Wang, Qianli Xing, and Zipei Fan. Tgrpo: Fine-tuning vision-language-action model via trajectory-wise group relative policy optimization. *arXiv preprint arXiv:2506.08440*, 2025.
- [10] Cheng Chi, Zhenjia Xu, Chuer Pan, Eric Cousineau, Benjamin Burchfiel, Siyuan Feng, Russ Tedrake, and Shuran Song. Universal manipulation interface: In-the-wild robot teaching without in-the-wild robots. *arXiv preprint arXiv:2402.10329*, 2024.
- [11] Hao-Shu Fang, Chenxi Wang, Hongjie Fang, Minghao Gou, Jirong Liu, Hengxu Yan, Wenhai Liu, Yichen Xie, and Cewu Lu. Anygrasp: Robust and efficient grasp perception in spatial and temporal domains. *IEEE Transactions on Robotics*, 2023.
- [12] Haoran Geng, Feishi Wang, Songlin Wei, Yuyang Li, Bangjun Wang, Boshi An, Charlie Tianyue Cheng, Haozhe Lou, Peihao Li, Yen-Jen Wang, et al. Roboverse: Towards a unified platform, dataset and benchmark for scalable and generalizable robot learning. *arXiv preprint arXiv:2504.18904*, 2025.
- [13] Chenyang Gu, Jiaming Liu, Hao Chen, Runzhong Huang, Qingpo Wu, Zhuoyang Liu, Xiaoqi Li, Ying Li, Renrui Zhang, Peng Jia, Pheng-Ann Heng, and Shanghang Zhang. Manualvla: A unified vla model for chain-of-thought manual generation and robotic manipulation, 2025. URL <https://arxiv.org/abs/2512.02013>.
- [14] Yanjiang Guo, Jianke Zhang, Xiaoyu Chen, Xiang Ji, Yen-Jen Wang, Yucheng Hu, and Jianyu Chen. Improving vision-language-action model with online reinforcement learning. *arXiv preprint arXiv:2501.16664*, 2025.
- [15] Tuomas Haarnoja, Aurick Zhou, Pieter Abbeel, and Sergey Levine. Soft actor-critic: Off-policy maximum entropy deep reinforcement learning with a stochastic actor. In *International conference on machine learning*, pages 1861–1870. Pmlr, 2018.
- [16] Dongchi Huang, Zhirui Fang, Tianle Zhang, Yihang Li, Lin Zhao, and Chunhe Xia. Co-rft: Efficient fine-tuning of vision-language-action models through chunked offline reinforcement learning. *arXiv preprint arXiv:2508.02219*, 2025.
- [17] Physical Intelligence, Kevin Black, Noah Brown, James Darpinian, Karan Dhabalia, Danny Driess, Adnan Esmail, Michael Equi, Chelsea Finn, et al.  $\pi_{0.5}$ : a vision-language-action model with open-world generalization,

2025. URL <https://arxiv.org/abs/2504.16054>.
- [18] Yueru Jia, Jiaming Liu, Shengbang Liu, Rui Zhou, Wanhe Yu, Yuyang Yan, Xiaowei Chi, Yandong Guo, Boxin Shi, and Shanghang Zhang. Video2act: A dual-system video diffusion policy with robotic spatio-temporal modeling. *arXiv preprint arXiv:2512.03044*, 2025.
- [19] Guangqi Jiang, Haoran Chang, Ri-Zhao Qiu, Yutong Liang, Mazeyu Ji, Jiyue Zhu, Zhao Dong, Xueyan Zou, and Xiaolong Wang. Gsworld: Closed-loop photo-realistic simulation suite for robotic manipulation. *arXiv preprint arXiv:2510.20813*, 2025.
- [20] Zhenyu Jiang, Yuqi Xie, Kevin Lin, Zhenjia Xu, Weikang Wan, Ajay Mandlekar, Linxi Jim Fan, and Yuke Zhu. Dexmimicgen: Automated data generation for bimanual dexterous manipulation via imitation learning. In *2025 IEEE International Conference on Robotics and Automation (ICRA)*, pages 16923–16930. IEEE, 2025.
- [21] Siddharth Karamcheti, Suraj Nair, Ashwin Balakrishna, Percy Liang, Thomas Kollar, and Dorsa Sadigh. Prismatic vlms: Investigating the design space of visually-conditioned language models. In *Forty-first International Conference on Machine Learning*, 2024.
- [22] Moo Jin Kim, Karl Pertsch, Siddharth Karamcheti, Ted Xiao, Ashwin Balakrishna, Suraj Nair, Rafael Rafailov, Ethan Foster, Grace Lam, Pannag Sanketi, et al. Openvla: An open-source vision-language-action model. *arXiv preprint arXiv:2406.09246*, 2024.
- [23] KIRI Innovations. KIRI Engine: 3D Scanner App for iPhone, Android, and Web. <https://www.kiriengine.app/>.
- [24] Kun Lei, Huanyu Li, Dongjie Yu, Zhenyu Wei, Lingxiao Guo, Zhennan Jiang, Ziyu Wang, Shiyu Liang, and Huazhe Xu. RI-100: Performant robotic manipulation with real-world reinforcement learning. *arXiv preprint arXiv:2510.14830*, 2025.
- [25] Kun Lei, Huanyu Li, Dongjie Yu, Zhenyu Wei, Lingxiao Guo, Zhennan Jiang, Ziyu Wang, Shiyu Liang, and Huazhe Xu. RI-100: Performant robotic manipulation with real-world reinforcement learning, 2025. URL <https://arxiv.org/abs/2510.14830>.
- [26] Haozhan Li, Yuxin Zuo, Jiale Yu, Yuhao Zhang, Zhao-hui Yang, Kaiyan Zhang, Xuekai Zhu, Yuchen Zhang, Tianxing Chen, Ganqu Cui, et al. Simplevla-rl: Scaling vla training via reinforcement learning. *arXiv preprint arXiv:2509.09674*, 2025.
- [27] Qixiu Li, Yaobo Liang, Zeyu Wang, Lin Luo, Xi Chen, Mozhen Liao, Fangyun Wei, Yu Deng, Sicheng Xu, Yizhong Zhang, et al. Cogact: A foundational vision-language-action model for synergizing cognition and action in robotic manipulation. *arXiv preprint arXiv:2411.19650*, 2024.
- [28] Xinhai Li, Jialin Li, Ziheng Zhang, Rui Zhang, Fan Jia, Tiancai Wang, Haoqiang Fan, Kuo-Kun Tseng, and Ruiping Wang. Robosim: A real2sim2real robotic gaussian splatting simulator, 2025. URL <https://arxiv.org/abs/2411.11839>.
- [29] Fanqi Lin, Ruiqian Nai, Yingdong Hu, Jiacheng You, Junming Zhao, and Yang Gao. Onetwovla: A unified vision-language-action model with adaptive reasoning. *arXiv preprint arXiv:2505.11917*, 2025.
- [30] Jiaming Liu, Mengzhen Liu, Zhenyu Wang, Pengju An, Xiaoqi Li, Kaichen Zhou, Senqiao Yang, Renrui Zhang, Yandong Guo, and Shanghang Zhang. Robomamba: Efficient vision-language-action model for robotic reasoning and manipulation. *Advances in Neural Information Processing Systems*, 37:40085–40110, 2024.
- [31] Jiaming Liu, Hao Chen, Pengju An, Zhuoyang Liu, Renrui Zhang, Chenyang Gu, Xiaoqi Li, Ziyu Guo, Sixiang Chen, Mengzhen Liu, et al. Hybridvla: Collaborative diffusion and autoregression in a unified vision-language-action model. *arXiv preprint arXiv:2503.10631*, 2025.
- [32] Jijia Liu, Feng Gao, Bingwen Wei, Xinlei Chen, Qingmin Liao, Yi Wu, Chao Yu, and Yu Wang. What can rl bring to vla generalization? an empirical study. *arXiv preprint arXiv:2505.19789*, 2025.
- [33] Songming Liu, Lingxuan Wu, Bangguo Li, Hengkai Tan, Huayu Chen, Zhengyi Wang, Ke Xu, Hang Su, and Jun Zhu. Rdt-1b: a diffusion foundation model for bimanual manipulation. *arXiv preprint arXiv:2410.07864*, 2024.
- [34] Zhuoyang Liu, Jiaming Liu, Hao Chen, Ziyu Guo, Chengkai Hou, Chenyang Gu, Jiale Yu, Xiangju Mi, Renrui Zhang, Zhengping Che, Jian Tang, Pheng-Ann Heng, and Shanghang Zhang. Lasto: Latent spatio-temporal chain-of-thought for robotic vision-language-action model, 2026. URL <https://arxiv.org/abs/2601.05248>.
- [35] Haozhe Lou, Yurong Liu, Yike Pan, Yiran Geng, Jianteng Chen, Wenlong Ma, Chenglong Li, Lin Wang, Hengzhen Feng, Lu Shi, Liyi Luo, and Yongliang Shi. Robo-gs: A physics consistent spatial-temporal model for robotic arm with hybrid representation, 2024. URL <https://arxiv.org/abs/2408.14873>.
- [36] Guanxing Lu, Wenkai Guo, Chubin Zhang, Yuheng Zhou, Haonan Jiang, Zifeng Gao, Yansong Tang, and Ziwei Wang. Vla-rl: Towards masterful and general robotic manipulation with scalable reinforcement learning. *arXiv preprint arXiv:2505.18719*, 2025.
- [37] Jianlan Luo, Perry Dong, Yuexiang Zhai, Yi Ma, and Sergey Levine. Rlif: Interactive imitation learning as reinforcement learning. *arXiv preprint arXiv:2311.12996*, 2023.
- [38] Jianlan Luo, Perry Dong, Yuexiang Zhai, Yi Ma, and Sergey Levine. Rlif: Interactive imitation learning as reinforcement learning, 2024. URL <https://arxiv.org/abs/2311.12996>.
- [39] Jianlan Luo, Charles Xu, Jeffrey Wu, and Sergey Levine. Precise and dexterous robotic manipulation via human-in-the-loop reinforcement learning. *Science Robotics*, 10(10):eads5033, 2025.
- [40] Russell Mendonca, Emmanuel Panov, Bernadette Bucher, Jiuguang Wang, and Deepak Pathak. Continuously improving mobile manipulation with autonomous real-

- world rl. *arXiv preprint arXiv:2409.20568*, 2024.
- [41] Octo Model Team, Dibya Ghosh, Homer Walke, Karl Pertsch, Kevin Black, Oier Mees, Sudeep Dasari, Joey Hejna, Charles Xu, Jianlan Luo, Tobias Kreiman, You Liang Tan, Dorsa Sadigh, Chelsea Finn, and Sergey Levine. Octo: An open-source generalist robot policy. <https://octo-models.github.io>, 2023.
- [42] Delin Qu, Haoming Song, Qizhi Chen, Yuanqi Yao, Xinyi Ye, Yan Ding, Zhigang Wang, JiaYuan Gu, et al. Spatialvla: Exploring spatial representations for visual-language-action model. *arXiv preprint arXiv:2501.15830*, 2025.
- [43] Rafael Rafailov, Archit Sharma, Eric Mitchell, Christopher D Manning, Stefano Ermon, and Chelsea Finn. Direct preference optimization: Your language model is secretly a reward model. *Advances in neural information processing systems*, 36:53728–53741, 2023.
- [44] Tim Schneider. franky: High-level control library for franka robots. <https://github.com/TimSchneider42/franky>, 2023. Software library. Python and C++ high-level control library for Franka robots, derived from the frankx project by Pantor.
- [45] John Schulman, Filip Wolski, Prafulla Dhariwal, Alec Radford, and Oleg Klimov. Proximal policy optimization algorithms. *arXiv preprint arXiv:1707.06347*, 2017.
- [46] Zhihong Shao, Peiyi Wang, Qihao Zhu, Runxin Xu, Junxiao Song, Xiao Bi, Haowei Zhang, Mingchuan Zhang, YK Li, Yang Wu, et al. Deepseekmath: Pushing the limits of mathematical reasoning in open language models. *arXiv preprint arXiv:2402.03300*, 2024.
- [47] Mohit Shridhar, Lucas Manuelli, and Dieter Fox. Perceiver-actor: A multi-task transformer for robotic manipulation. In *Proceedings of the 6th Conference on Robot Learning (CoRL)*, 2022.
- [48] Yifei Su, Ning Liu, Dong Chen, Zhen Zhao, Kun Wu, Meng Li, et al. Freqpolicy: Efficient flow-based visuomotor policy via frequency consistency. *arXiv preprint arXiv:2506.08822*, 2025.
- [49] Ioan A. Şucan et al. The Open Motion Planning Library. *IEEE Robotics & Automation Magazine*, 19(4):72–82, December 2012. doi: 10.1109/MRA.2012.2205651. <https://ompl.kavrakilab.org>.
- [50] Shuhan Tan, Kairan Dou, Yue Zhao, and Philipp Krähenbühl. Interactive post-training for vision-language-action models. *arXiv preprint arXiv:2505.17016*, 2025.
- [51] Marcel Torne, Arhan Jain, Jiayi Yuan, Vidaaranya Macha, Lars Ankile, Anthony Simeonov, Pulkit Agrawal, and Abhishek Gupta. Robot learning with super-linear scaling. *arXiv preprint arXiv:2412.01770*, 2024.
- [52] Marcel Torne, Anthony Simeonov, Zechu Li, April Chan, Tao Chen, Abhishek Gupta, and Pulkit Agrawal. Reconciling reality through simulation: A real-to-sim-to-real approach for robust manipulation. *arXiv preprint arXiv:2403.03949*, 2024.
- [53] Peng Wang, Shuai Bai, Sinan Tan, Shijie Wang, Zhihao Fan, Jinze Bai, Keqin Chen, Xuejing Liu, Jialin Wang, Wenbin Ge, et al. Qwen2-vl: Enhancing vision-language model’s perception of the world at any resolution. *arXiv preprint arXiv:2409.12191*, 2024.
- [54] Junjie Wen, Minjie Zhu, Yichen Zhu, Zhibin Tang, Jinming Li, Zhongyi Zhou, Chengmeng Li, Xiaoyu Liu, Yaxin Peng, Chaomin Shen, et al. Diffusion-vla: Scaling robot foundation models via unified diffusion and autoregression. *arXiv preprint arXiv:2412.03293*, 2024.
- [55] Junjie Wen, Yichen Zhu, Jinming Li, Minjie Zhu, Zhibin Tang, Kun Wu, Zhiyuan Xu, Ning Liu, Ran Cheng, Chaomin Shen, et al. Tinyvla: Towards fast, data-efficient vision-language-action models for robotic manipulation. *IEEE Robotics and Automation Letters*, 2025.
- [56] Mingdong Wu, Lehong Wu, Yizhuo Wu, Weiyao Huang, Hongwei Fan, Zheyuan Hu, Haoran Geng, Jinzhou Li, Jiahe Ying, Long Yang, et al. Simlauncher: Launching sample-efficient real-world robotic reinforcement learning via simulation pre-training. In *2025 IEEE/RSJ International Conference on Intelligent Robots and Systems (IROS)*, pages 7933–7940. IEEE, 2025.
- [57] Xiuwei Xu, Angyuan Ma, Hankun Li, Bingyao Yu, Zheng Zhu, Jie Zhou, and Jiwen Lu. R2rgen: Real-to-real 3d data generation for spatially generalized manipulation, 2025. URL <https://arxiv.org/abs/2510.08547>.
- [58] Zhengrong Xue, Shuying Deng, Zhenyang Chen, Yixuan Wang, et al. Demogen: Synthetic demonstration generation for data-efficient visuomotor policy learning. *arXiv preprint arXiv:2502.16932*, 2025.
- [59] Sizhe Yang, Wenye Yu, Jia Zeng, Jun Lv, Kerui Ren, Cewu Lu, Dahua Lin, and Jiangmiao Pang. Novel demonstration generation with gaussian splatting enables robust one-shot manipulation, 2025. URL <https://arxiv.org/abs/2504.13175>.
- [60] Weirui Ye, Fangchen Liu, Zheng Ding, Yang Gao, Oleh Rybkin, and Pieter Abbeel. Video2policy: Scaling up manipulation tasks in simulation through internet videos. *arXiv preprint arXiv:2502.09886*, 2025.
- [61] Justin Yu, Letian Fu, Huang Huang, Karim El-Refai, Rares Andrei Ambrus, Richard Cheng, Muhammad Zubair Irshad, and Ken Goldberg. Real2render2real: Scaling robot data without dynamics simulation or robot hardware. *arXiv preprint arXiv:2505.09601*, 2025.
- [62] Yang Yue, Zhiqi Chen, Rui Lu, Andrew Zhao, Zhaokai Wang, Shiji Song, and Gao Huang. Does reinforcement learning really incentivize reasoning capacity in llms beyond the base model? *arXiv preprint arXiv:2504.13837*, 2025.
- [63] Yanjie Ze, Gu Zhang, Kangning Zhang, Chenyuan Hu, Muhan Wang, and Huazhe Xu. 3d diffusion policy. *arXiv preprint arXiv:2403.03954*, 2024.
- [64] Hongyin Zhang, Zifeng Zhuang, Han Zhao, Pengxiang Ding, et al. Reinbot: Amplifying robot visual-language manipulation with reinforcement learning. *arXiv preprint arXiv:2505.07395*, 2025.
- [65] Zijian Zhang, Kaiyuan Zheng, Zhaorun Chen, Joel

Jang, Yi Li, Siwei Han, Chaoqi Wang, Mingyu Ding, Dieter Fox, and Huaxiu Yao. Grape: Generalizing robot policy via preference alignment. *arXiv preprint arXiv:2411.19309*, 2024.

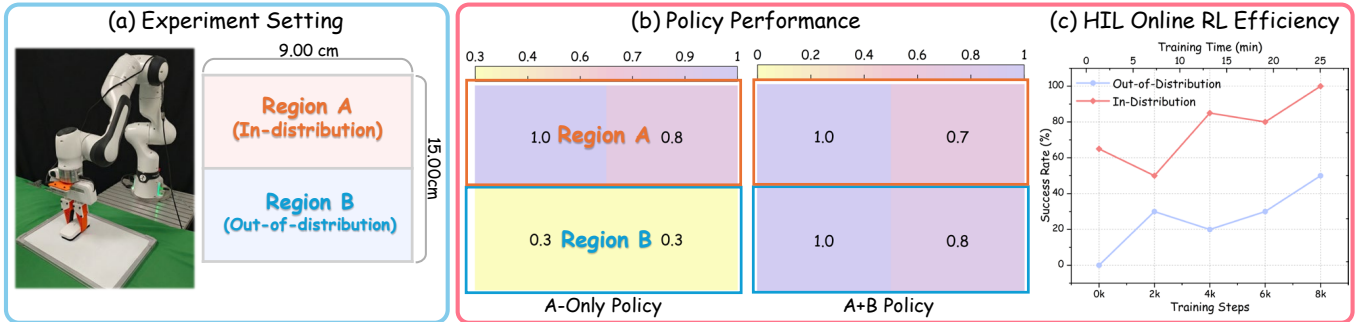


Fig. 8: **Motivation.** (a) We split the workspace into an in-distribution region (A) and an out-of-distribution region (B), defined by the manipulated object’s center location at task completion. (b) Heatmaps visualize the success rate of different policies. (c) Learning curves show the online RL training dynamics of the A-only policy in both regions.

## APPENDIX

### A. ADDITIONAL MOTIVATION EXPERIMENTS

Similar to the motivating observation in the main text, and motivated by the general-domain study [62], we establish an analogous finding in robotic manipulation: exploration in real-world VLA RL is effectively constrained by the spatial support of the trajectory distribution induced during SFT. As shown in Fig. 8 (a), beyond the main text, we further validate this phenomenon on the *Erase-Whiteboard* task and identify a dual bottleneck: (1) it limits the set of states that can be reliably explored, and (2) it substantially reduces online RL efficiency, even with human intervention.

**Experimental Setup.** The experimental setup is identical to that in Section III-B. We use the same criterion to split the workspace into an in-distribution Region A and an out-of-distribution Region B that is not observed during SFT. Below, we present the motivation results on the *Erase-Whiteboard* task.

**Bottleneck I.** We compare two SFT data distributions with different spatial coverage: (i) **A-only**, with 30 real-world demonstrations from Region A, and (ii) **A+B**, which augments A-only with 30 digital-twin demonstrations from Region B. We first evaluate the spatial generalization of the resulting SFT policies. We then initialize online RL from the A-only SFT policy and run autonomous training in the previously unseen Region B to assess how demonstration coverage shapes the effective exploration space.

**Findings I.** As shown in Fig. 8 (b), the success-rate heatmaps show a clear coverage-induced generalization gap. The **A-only** policy achieves high success within Region A but fails almost everywhere in Region B, indicating limited spatial extrapolation to uncovered configurations. In contrast, the **A+B** policy not only preserves strong performance in Region A, but also substantially improves success in Region B. More importantly, running autonomous online RL in Region B from the A-only initialization results in a clear exploration deadlock: when started from OOD configurations, the policy fails to reliably obtain positive rewards even after two hours of training. These results corroborate that the effective exploration space

is tightly bounded by the spatial support of the trajectory distribution induced during SFT: without Region B coverage, the policy struggles to produce reward-yielding behaviors when initialized in OOD states, leading to exploration stall.

**Bottleneck II.** To alleviate the exploration deadlock, we follow prior real-world RL methods [39, 8] and use Human-in-the-Loop (HiL) intervention to guide the robot toward successful task completion. However, it remains unclear whether human guidance alone guarantees efficient online adaptation in OOD settings. To investigate this, we compare two regimes: In-distribution post-training, where online RL is performed in the familiar Region A, and OOD post-training, where online RL is conducted in the unfamiliar Region B. All models are initialized from the same A-only SFT policy, and HiL intervention is applied in both regimes.

**Findings II.** The learning curves reveal a pronounced sample-efficiency disparity. In-distribution post-training improves rapidly and reaches a high success rate with limited interaction, whereas OOD post-training increases much more slowly and exhibits noticeably larger instability under the same budget, failing to match the in-distribution performance. These results suggest that, even with HiL, learning in the previously unseen Region B remains difficult because the replay buffer becomes highly imbalanced (across ID vs. OOD samples, teleoperation vs. RL trajectory styles, and successful vs. failed episodes), leading to inefficient and unstable gradient updates..

**Conclusion.** Overall, the additional motivation experiments echo the dual exploration bottlenecks observed in Sec. III-B: (1) exploration coverage is constrained by the spatial support of SFT, and (2) online adaptation in OOD settings is markedly less sample-efficient. These observations further motivate TwinRL to introduce digital twins to expand exploration coverage *before* real-world interaction and systematically improve online learning efficiency.

### B. REAL-WORLD SET-UP

The real-world deployment of TwinRL is built on a modular robotic platform designed to support precise manipulation and efficient online reinforcement learning (RL) with reduced human intervention. All experiments are conducted on a 7-DoF

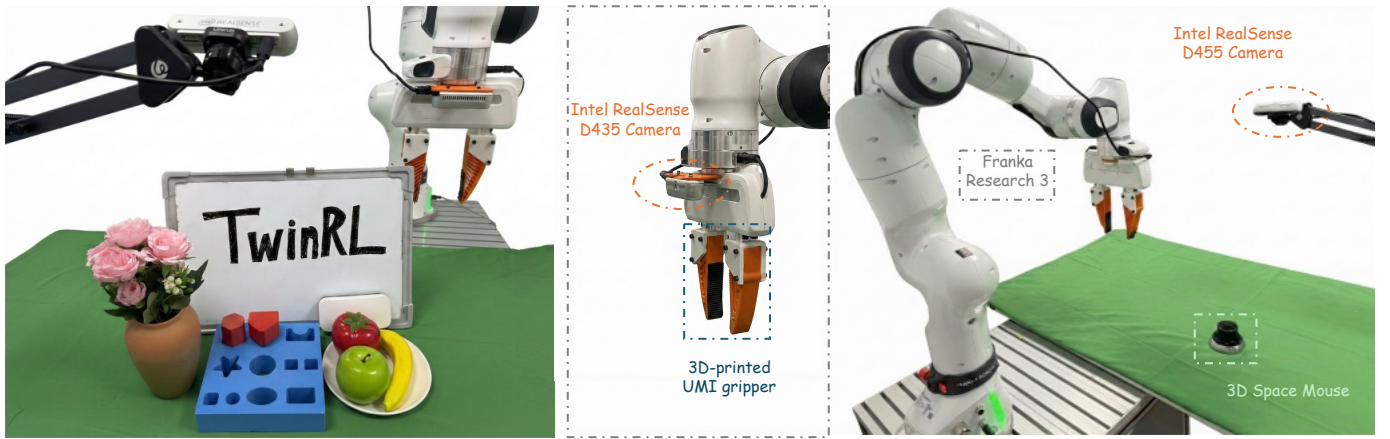


Fig. 9: Real-World Robot Setups and Experimental Assets.

Franka Emika Research 3 (FR3) robotic arm equipped with the 3D-printed UMI gripper [10], enabling accurate Cartesian end-effector control for contact-rich, precision manipulation tasks. As shown in Fig. 9, we employ a dual-camera sensing setup to provide rich visual feedback for both perception and control. A fixed third-person RGB camera (Intel RealSense D455) captures a global view of the workspace, while a wrist-view RGB camera (Intel RealSense D435) is attached to the end effector to provide close-range observations. At each timestep, the observation consists of two RGB images: one from the wrist-view camera (resized to  $128 \times 128$ ) and one from the third-person camera (resized to  $256 \times 256$ ).

All real-world demonstrations and human-in-the-loop (HiL) interactions are collected via teleoperation using a 3D Space-Mouse, which enables operators to provide high-quality expert trajectories as well as targeted corrective interventions during online learning. To ensure a fair comparison, all methods are evaluated using identical hardware, sensing, and control software [44]. The actor and learner processes for real-world online RL run on a workstation equipped with an NVIDIA GeForce RTX 4090 GPU, supporting policy inference and asynchronous training. The supervised fine-tuning (SFT) stage is performed offline on a server equipped with NVIDIA A100 GPUs (80GB).

### C. ADDITIONAL DETAILS OF THE DIGITAL TWIN

In this section, we provide additional implementation details of our digital twin construction and object-centric modeling.

*a) Digital Twin Construction.*: The digital twin is instantiated from casually captured smartphone videos. Specifically, we record a single video of approximately one minute by moving a handheld smartphone around the target scene, ensuring full coverage of the robot workspace, including the complete robot base and surrounding environment. The video is captured at 30 FPS with a resolution of  $1080 \times 1920$ . The extracted frames are used to reconstruct the static scene geometry via 3D Gaussian Splatting (3DGS) tool [23].

Following [59], to automate the alignment of the digital twin with the real-world setup, we anchor the coordinate trans-

formation to URDF-defined robot frames. We first obtain a coarse initialization using point-cloud-based registration (e.g., ICP [2]). However, even after the coarse point-cloud-based alignment, residual misalignment may still remain, which can lead to inconsistencies between geometric alignment and visual appearance. To mitigate this issue, we re-implement the differentiable 3DGS rendering method and use it to refine the alignment. Specifically, we select  $N$  camera viewpoints and, for each view, render a binary segmentation mask from the robot URDF model, denoted as  $\mathcal{I}_i^{\text{URDF}}$ , as well as a segmentation mask rendered from the robot’s 3D Gaussian representation under the current transformation, denoted as  $\mathcal{I}_i^{\text{GS}}$ . Pixels corresponding to the robot are assigned a value of 1, and all other pixels are set to 0. The alignment objective is defined as the mean pixel-wise discrepancy between the two masks across all viewpoints:

$$\mathcal{L}_{\text{align}} = \frac{1}{N} \sum_{i=1}^N (\mathcal{I}_i^{\text{URDF}} - \mathcal{I}_i^{\text{GS}})^2. \quad (7)$$

Starting from the ICP-based initialization, we parameterize the relative transformation—including translation, rotation, and scale—as  $\hat{T}_{\text{rel}}$ . Using differentiable rendering, the robot 3D Gaussian model  $\hat{g}_{\text{robot}}$  is rendered from each camera viewpoint after applying  $\hat{T}_{\text{rel}}$ , yielding the following optimization objective:

$$\mathcal{I}_i^{\text{GS}} = \text{Render}(\hat{g}_{\text{robot}} \circ \hat{T}_{\text{rel}, \text{Camera}_i}). \quad (8)$$

By exploiting the differentiability of 3DGS, we optimize  $\hat{T}_{\text{rel}}$  via backpropagation and gradient descent, resulting in a refined alignment that enforces both geometric and visual consistency between the reconstructed robot and the real-world coordinate frame.

*b) Object-Centric Pose Estimation.*: We adopt an object-centric representation to model the manipulated object and its interaction with the robot. Given RGB observations, the target object is first reconstructed using SAM3D [7], producing a dense 3D representation of the object geometry. The reconstructed object is then uniformly subsampled to a fixed

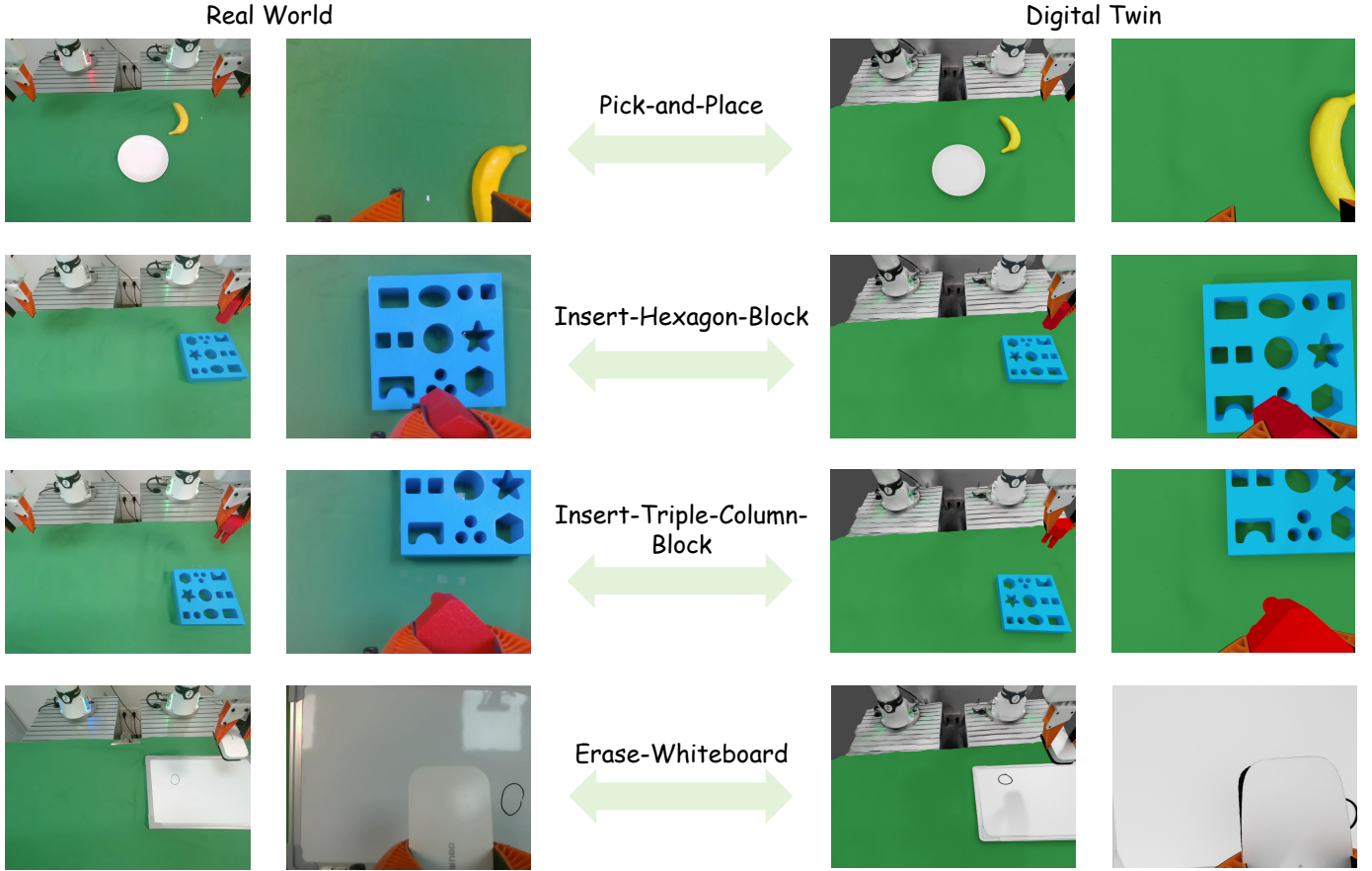


Fig. 10: Qualitative comparison between real-world scenarios and their corresponding digital-twin renderings.

number (100k) of points to form an object-centric point cloud. We augment the object point cloud with a planar point cloud representing the supporting tabletop beneath the object. The combined point cloud is fed into AnyGrasp [11], which returns grasp hypotheses ranked by confidence. We then select the top- $n$  candidates, each represented as a 6-DoF grasp pose in the object-centric coordinate frame. After initializing the object pose and its 6-DoF trajectory in the scene, we leverage the frame alignment results to transform these object-centric grasp poses into the robot coordinate system. Specifically, the estimated relative transformation between the reconstructed scene and the real-world robot base frame enables us to compute the time-varying end-effector poses in the robot base frame. As a result, both the robot motion and the object trajectory are consistently defined within a shared coordinate frame in the digital twin.

*c) Trajectory Generation and Assembly:* To generate diverse and task-consistent trajectories, we systematically vary the object’s initial configurations, target poses, and motion paths within the digital twin. Following previous work [47], for each task, we extract a set of keyframes corresponding to critical stages of manipulation. Each keyframe specifies an object pose, from which the corresponding grasp pose and end-effector pose can be derived. We consider two complementary

approaches for trajectory generation:

**Motion-Planning-Based Trajectory Generation.** Given the object poses at the keyframes, we directly employ motion planning toolkits [49] to generate collision-free and kinematically feasible end-effector trajectories that connect the corresponding grasp poses. This approach ensures geometric consistency and feasibility under kinematic constraints.

**Demonstration-Based Trajectory Augmentation.** We leverage a single human teleoperated demonstration trajectory  $\tau = \{\mathbf{x}_t\}_{t=0}^{T-1}$ ,  $\mathbf{x}_t \in \mathbb{R}^7$ , where  $T$  denotes the trajectory length, and each state  $\mathbf{x}_t = (x_t, y_t, z_t, r_t, p_t, y_t, g_t)$  consists of the end-effector position, orientation (roll-pitch-yaw) and gripper state. To synthesize new execution trajectories, we utilize the trajectory interpolation scheme from [61]. For the translational component, we compute an affine transformation that jointly aligns the start and end poses of the original teleoperated trajectory to the desired target start and end poses, and apply this transformation to the translational component of the entire trajectory. For the rotational component, we interpolate end-effector orientations along the trajectory using spherical linear interpolation, ensuring smooth and continuous rotation.

Finally, given the object and end-effector trajectories, the corresponding robot and object 3D assets are assembled in the digital twin through kinematic transformations and rendered to produce paired visual observations and robot states for subse-

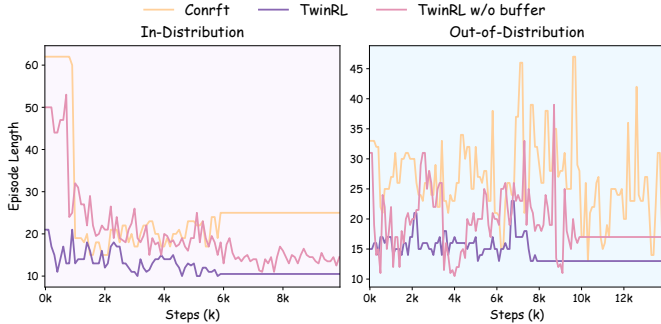


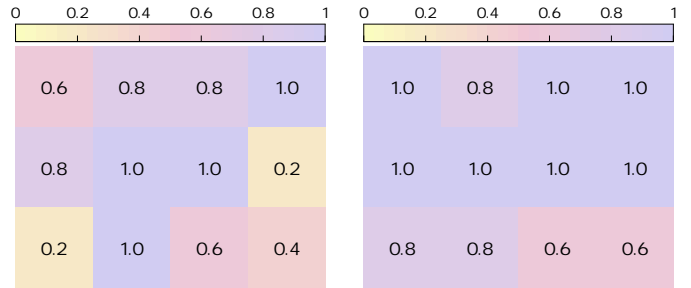
Fig. 11: **Episode length.** We report episode length curves for online RL in insert-triple-column-block manipulation tasks under both ID and OOD settings. The y-axis shows episode length, and the x-axis reports our model training steps.

quent policy learning. A qualitative comparison between real-world executions and their digital-twin renderings is shown in Fig. 10.

#### D. ADDITIONAL RESULTS

**Episode Length.** We provide additional analysis using episode length to characterize the efficiency of real-world online reinforcement learning. All experiments are conducted on the Insert-Triple-Column-Block task under both in-distribution (ID) and out-of-distribution (OOD) settings, following the same real-world training protocol and baselines as in Section IV-B of the main paper. In this study, episode length is measured as the total number of low-level control steps executed within an episode, which terminates upon success, failure, or reaching a predefined step limit. Fig. 11 reports episode length as a function of real-world training time and training steps for all methods. Across both ID and OOD regions, all methods exhibit a gradual reduction in episode length as training progresses, indicating that online reinforcement learning gradually leads to more direct and efficient execution patterns. **In ID regions**, TwinRL demonstrates a markedly faster reduction in episode length, suggests that twin-guided exploration provides more informative warm-up and early online rollouts, allowing the policy to focus on high-value state-action sequences and avoid redundant corrective motions. **In OOD regions**, the difference becomes more pronounced. Baseline methods often require substantially longer episodes throughout training, indicating inefficient exploration and repeated recovery behaviors when encountering configurations outside the SFT data distribution. Comparing TwinRL with TwinRL w/o buffer further highlights the role of the twin replay buffer. While TwinRL w/o buffer already benefits from twin-guided exploration, TwinRL achieves shorter episode lengths earlier and with greater stability, indicating that initializing real-world training with twin RL rollouts helps bridge the offline-to-online transition and mitigates inefficient early exploration.

**Additional Ablation Study:** We conduct an additional ablation study on the Insert-Hexagon-Block task to further



(a) OOD-only augmentation

(b) Joint augmentation

Fig. 12: **Additional ablations.** We evaluate how augmenting SFT with digital-twin data affects performance, comparing (a) adding twin data only in the OOD region and (b) adding twin data in both the ID and OOD regions. Each grid cell is evaluated with five rollout trials.

examine how the distribution of twin data affect warm-up SFT performance. In this study, we fix the amount of real-world data to 30 in-distribution (ID) trajectories and assess whether allocating synthetic twin trajectories within the ID region improves alignment between real-world and digital-twin domains. Specifically, we compare two settings: OOD-only augmentation (ID 0 / OOD 30) and joint augmentation (ID 30 / OOD 30). Fig. 12 reports the corresponding success-rate heatmaps, where each grid cell is evaluated with five rollout trials. Compared to OOD-only augmentation, jointly augmenting both ID and OOD regions leads to more consistent and uniformly higher success rates across the workspace. While adding twin data in the OOD region already helps expand the exploration space and improves performance in previously uncovered areas, augmenting the ID region further improves performance, particularly within the in-distribution region. These results suggest that, beyond expanding coverage, including twin data in the in-distribution region helps reduce the gap between synthetic and real data, yielding a more reliable warm-up policy.

**Evaluation in the Digital Twin:** To quantitatively assess how well the digital twin captures the real-world task difficulty landscape, we conduct a controlled evaluation under matched initial configurations. This landscape fidelity is critical for TwinRL’s exploration space expansion and sim-to-real guided exploration, so we compare task success rates between real-world and digital-twin executions. We focus on the Insert-Hexagon-Block task and evaluate the SFT checkpoint trained with mixed real-world and digital-twin data, before any online reinforcement learning is performed. The task workspace is discretized into in-distribution and out-of-distribution grids, identical to those used in the real-world evaluation. For each grid cell, the same policy is evaluated for 5 rollouts, both on the physical robot and in the corresponding digital-twin environment. Fig. 13 reports the resulting success-rate heatmaps for real-world execution and digital twin execution. The results show that the digital twin accurately reflects the global structure of task difficulty observed in the real world.

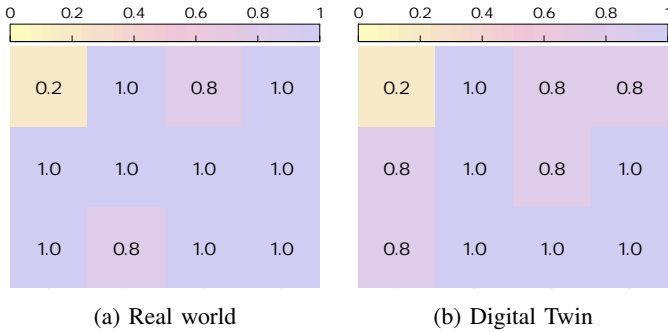


Fig. 13: Comparison of success-rate heatmaps between the real-world scenario and the corresponding digital-twin scenario using the same SFT model on the Insert-Hexagon-Block task.

Although absolute success rates in the digital twin may differ from those in the real world, the relative ordering of easy versus difficult regions is well preserved. As a result, sampling and prioritizing these configurations during twin-based rollouts effectively identifies informative states for subsequent real-world exploration. These results demonstrate that digital twins in TwinRL function not merely as simulators, but as effective exploration amplifiers and guides, enabling systematic identification of challenging configurations and improving the efficiency of real-world reinforcement learning.

**Additional Robustness Evaluation:** To further evaluate our approach’s generalization capability beyond the insertion task, we extend the zero-shot robustness evaluation to the Pick-and-Place task. Consistent with the analysis in Section IV-D, we compared the SFT policy and the TwinRL-guided policy in three categories of previously unseen environmental perturbations: Background (introduction of distractors and clutter), Darker lighting (low-light conditions), and Dynamic lighting (changing colored light patterns). As shown in Fig. 14, the results of the Pick-and-Place task align with our previous findings. The SFT baseline shows significant performance degradation under distribution shifts, particularly during the grasping phase, where background clutter causes visual ambiguity. In contrast, the TwinRL policy demonstrates remarkable resilience, maintaining a high success rate with only a slight decrease in performance compared to the original environment. These results further corroborate that TwinRL does not merely memorize visual features from demonstrations. Rather, the twin-guided HiL mechanism effectively directs the policy to explore and recover from high-risk states. This fosters the learning of robust, noise-tolerant decision boundaries, which are critical for robotic manipulation.

**Real-World Visualizations:** Fig. 15 illustrates representative task executions across all four of our tasks including Pick-and-Place, Insert-Hexagon-Block, Insert-Triple-Column-Block and Erase-Whiteboard in single-arm settings. We observe that TwinRL produces smooth and continuous motions, especially for precise actions such as insertion.

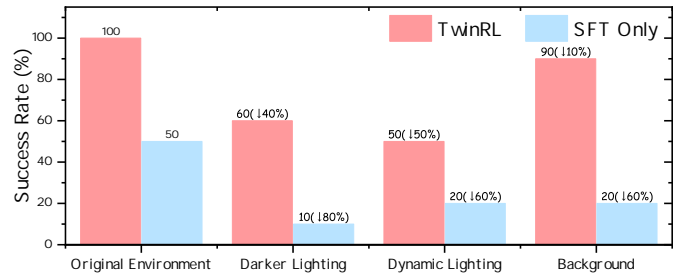


Fig. 14: **Additional Robustness Evaluation.** We additionally compare the SFT policy and the TwinRL-guided online RL policy on the Pick-and-Place task under previously unseen environmental perturbations.

## E. FAILURE CASE ANALYSIS

In the four tasks designed for this study, several typical failure modes were identified. As shown in Figure. 16, the main objects and regions where issues occurred are highlighted with red boxes, and the causes of failure are analyzed below.

**Imprecise Object Detection:** In the Pick-and-Place task, the model is required to accurately grasp a banana from various positions on the table and place it onto a plate. However, during this process, the robotic arm collides with the banana as it descends, causing the object to shift and resulting in a failure to grasp. This issue is particularly prominent in the data augmentation regions but improves as the online reinforcement learning (RL) progresses.

**Positional Instability:** In the Insertion tasks (Task 2 and Task 3), the robotic arm is required to insert a block with precision into a designated slot on the board, with the error constrained to within 2 millimeters. However, given the extensive task scope and stringent precision requirements, the robotic arm may encounter friction with the board while reaching certain distant positions. This friction results in the block’s loss of proper alignment, either in terms of angle or position, thereby preventing it from achieving the correct placement. Consequently, variations in insertion angle and position inevitably arise, culminating in task failure.

**Manipulation height:** In the Erase-Whiteboard task, the FR3 robotic arm is assigned the task of utilizing an eraser to remove a predetermined pattern from a whiteboard. However, the robotic arm sometimes fails to reach the required height for effective erasure, resulting in improper alignment of the eraser with the whiteboard surface and incomplete erasure. Moreover, the absence of visual feedback during task execution hinders the system’s capacity to ascertain in real-time whether the pattern has been fully erased, thereby elevating the probability of failure.

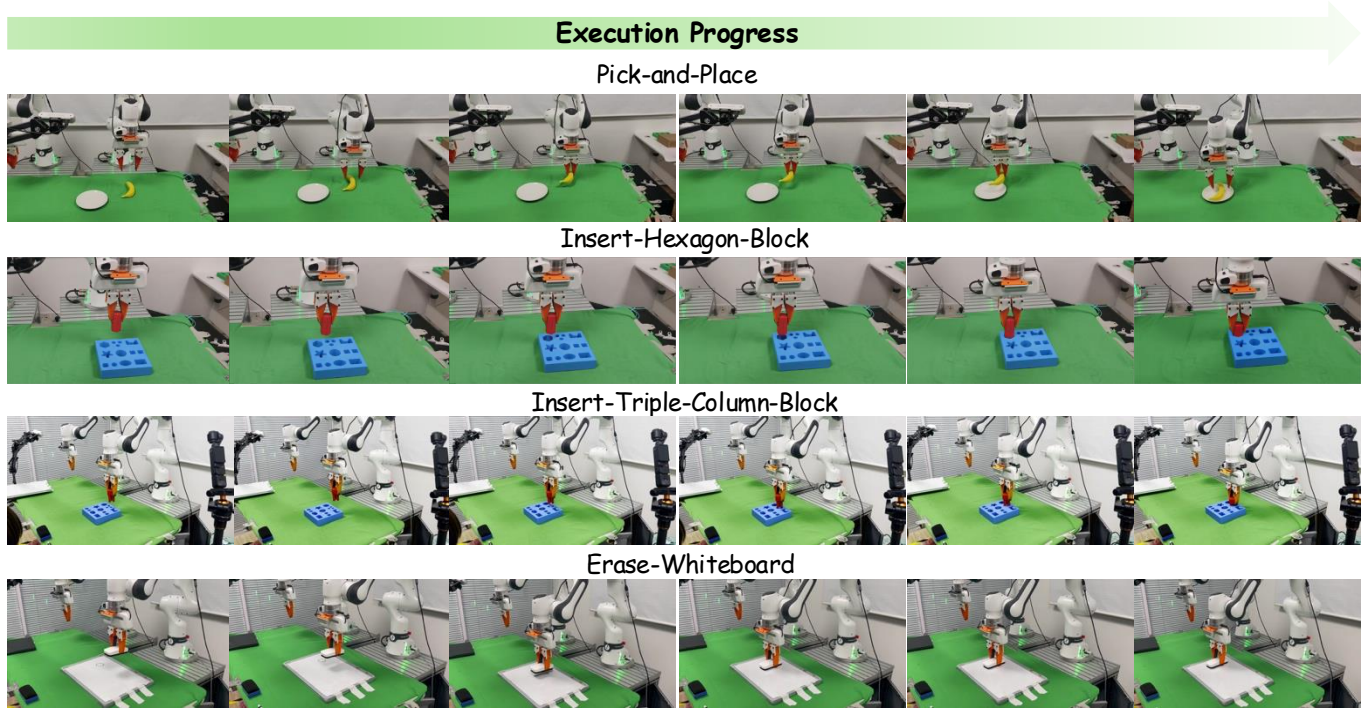


Fig. 15: Visualization of complete real-world task execution processes (left to right).

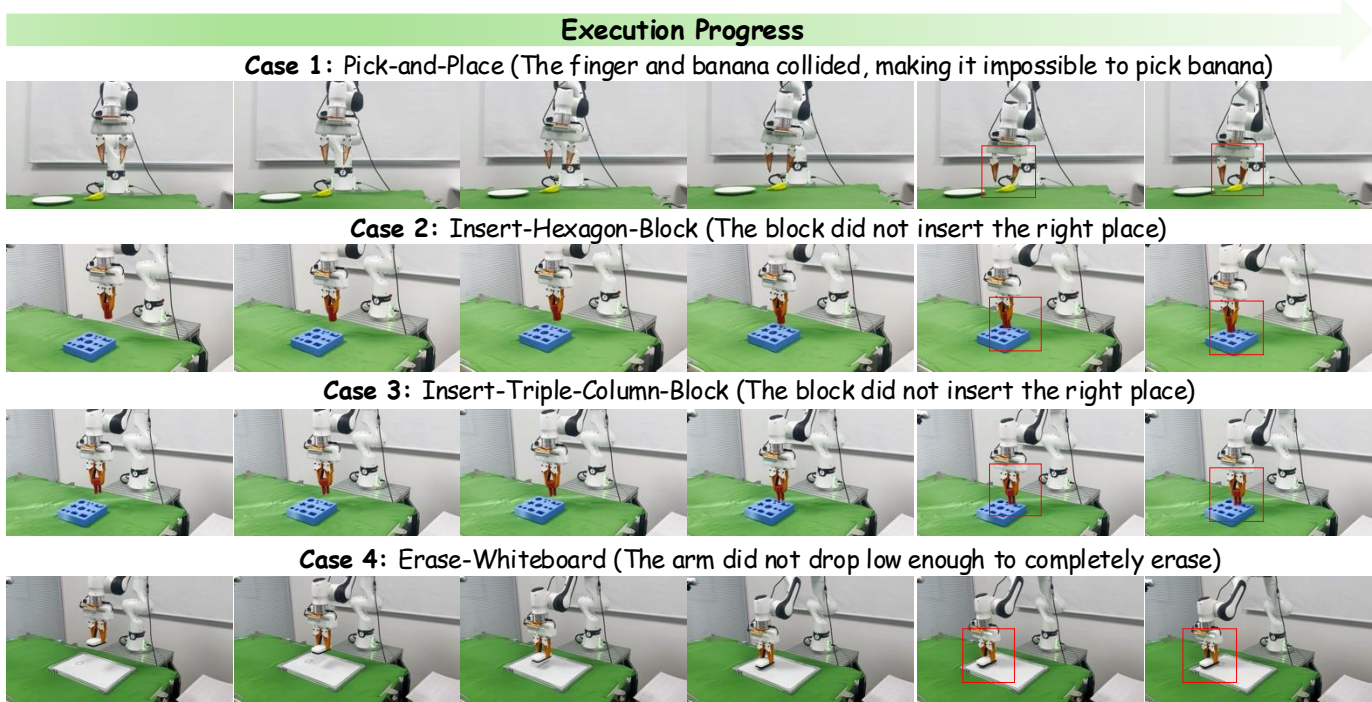


Fig. 16: Visualization of failure cases on different tasks, and red box highlights the failure positions.